PCCP

Li-Ion Hopping Conduction in Highly Concentrated Lithium Bis(fluorosulfonyl)amide/Dinitrile Liquid Electrolytes

Journal:	*Physical Chemistry Chemical Physics*
Manuscript ID	CP-ART-04-2019-001839.R1
Article Type:	Paper
Date Submitted by the Author:	25-Apr-2019
Complete List of Authors:	Ugata, Yosuke; Yokohama National University, Department of Chemistry and Biotechnology Thomas, Morgan; Sophia University, MANDAI, Toshihiko; Iwate Daigaku, mandai@iwate-u.ac.jp Ueno, Kazuhide; Yokohama National University, Department of Chemistry and Biotechnology Dokko, Kaoru; Yokohama National University, Department of Chemistry and Biotechnology Watanabe, Masayoshi; Yokohama National University, Chemistry andBiotechnology

Li-Ion Hopping Conduction in Highly Concentrated Lithium Bis(fluorosulfonyl)amide/Dinitrile Liquid Electrolytes

Yosuke Ugata,[a] Morgan L. Thomas,[a,§] Toshihiko Mandai,[b,c] Kazuhide Ueno,[a] Kaoru Dokko,[a,d,*] and Masayoshi Watanabe [a]

[a] Department of Chemistry and Biotechnology, Yokohama National University, 79-5 Tokiwadai, Hodogaya-ku, Yokohama 240-8501, Japan

[b] Department of Chemistry and Biological Science Studies in Chemistry, Iwate University, Ueda 4-3-5, Morioka, 020-8551, Japan

[c] Center for Green Research on Energy and Environmental Materials, National Institute of Materials Science, 1-1 Namiki, Tsukuba, Ibaraki 305-0044, Japan

[d] Unit of Elements Strategy Initiative for Catalysts & Batteries (ESICB), Kyoto University, Kyoto 615-8510, Japan

[§] Present address: Department of Materials and Life Sciences, Faculty of Science and Engineering, Sophia University, 7-1 Kioicho, Chiyoda-ku, Tokyo 102-8554, Japan

* CORRESPONDING AUTHOR FOOTNOTE: To whom correspondence should be addressed.

E-mail: dokko-kaoru-js@ynu.ac.jp

ABSTRACT

Li^+ ion hopping conduction in highly concentrated solutions of lithium bis(fluorosulfonyl)amide (LiFSA) dissolved in dinitrile solvents, namely succinonitrile, glutaronitrile, and adiponitrile, was investigated. Phase behaviors of the LiFSA/dinitrile binary mixtures assessed by differential scanning calorimetry suggested that LiFSA and the dinitriles form stable solvates in a molar ratio of 1:2. For succinonitrile, a glass forming room temperature liquid is formed when [LiFSA]/[succinonitrile] > 1. The corresponding glutaronitrile and adiponitrile mixtures have melting points below 60 °C. The self-diffusion coefficients of Li^+, FSA^-, and dinitrile measured with pulsed field gradient NMR suggested that Li^+ ion diffuses faster than anion and dinitrile in the liquids of composition [LiFSA]/[dinitrile] = 1/0.8, indicating emergence of Li^+ ion hopping conduction. X-ray crystallography for the LiFSA-$(dinitrile)_2$ solvates and Raman spectroscopy for the liquids with composition [LiFSA]/[dinitrile] > 1 revealed that the two cyano groups of the dinitrile coordinate to two different Li^+ ions and form solvent-bridged structures of (Li^+−dinitrile−Li^+). In addition, the Raman spectra suggested that ionic aggregates (Li^+−FSA^-−Li^+) are formed in the liquids with composition [LiFSA]/[dinitrile] > 1. Although there is frequent ligand (dinitrile and/or anion) exchange for each Li^+ ion in the liquid state, the polymeric network structures (solvent-bridged structure and ionic aggregates) restrict the facile motion of ligands because each ligand is interacting with multiple Li^+ ions in the highly concentrated electrolytes. This induces the faster diffusion of the Li^+ ion than that of the ligands, i.e., hopping conduction of Li^+ through ligand exchange. Electrochemical measurements clarified that the [LiFSA]/[succinonitrile] = 1/0.8 electrolyte possesses a relatively high Li^+ transport ability (limiting current density > 7 mA cm^{-2}) thanks to the Li^+ hopping conduction, regardless of its extremely high viscosity (3142 mPa s) and relatively low conductivity (0.26 mS cm^{-1}) at room temperature. Furthermore, this electrolyte was shown to have a high

Li^+ transference number (>0.6), exhibited reversible Li metal deposition/dissolution i.e. suppression of reductive decomposition of the solvent, and could be successfully applied to graphite and $LiNi_{1/3}Mn_{1/3}Co_{1/3}O_2$ half-cells.

INTRODUCTION

The cyano groups of nitriles have relatively high polarity, derived from the lone pair on the nitrogen atom. The cyano group can coordinate to metal ions and can dissociate alkali metal salts into ions through the coordination, i.e., solvation. Therefore, low molecular weight nitriles have been widely employed as aprotic electrolyte solvents for electrolyte salts in the field of electrochemistry.[1] Acetonitrile (AN) is known to have relatively high oxidative stability and has been investigated as an electrolyte solvent for high voltage lithium batteries.[2,3] In addition, succinonitrile (SN), which is a dinitrile having two cyano groups in its molecular structure, is known to have a plastic crystalline phase even with dissolved Li salts and has been investigated as a solid electrolyte for lithium batteries.[4–7] However, the reductive stability of nitrile-based electrolytes is poor. Nitriles easily decompose on the Li metal surface and have not been used in practical Li-ion batteries.[8] In 2013, Yamada et al. reported that reversible Li metal deposition/dissolution is possible in highly concentrated lithium bis(trifluoromethanesulfonyl)amide (LiTFSA)/AN solutions (> 4 mol dm^{-3}).[2] The reversible Li^+ intercalation into a graphite electrode was also demonstrated in 4.5 mol dm^{-3} lithium bis(fluorosulfonyl)amide (LiFSA)/AN electrolyte. Subsequently, they reported that highly concentrated NaFSA/SN electrolytes enable highly reversible Na^+ insertion into a hard carbon electrode.[9] These reports suggest that the reductive instability of the nitrile-based electrolytes can be overcome by increasing the concentration of alkali metal salts.

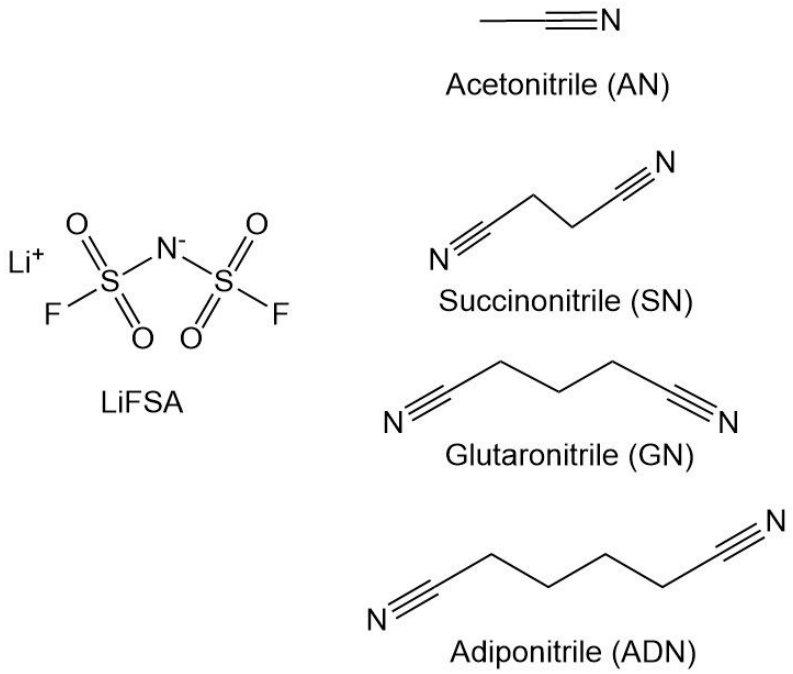

Figure 1. Chemical structures of LiFSA and nitrile solvents.

Here we report a unique Li^+ ion transport process in the highly concentrated electrolytes composed of LiFSA and dinitrile solvents, SN, glutaronitrile (GN), and adiponitrile (ADN). In this study, we investigated the solvate structures and transport properties of highly concentrated electrolytes composed of LiFSA and the dinitrile solvents (**Figure 1**). Dinitriles are equipped with two cyano groups and are expected to be able to interact with two different Li^+ ions when the Li salt concentration is high in the solution. Recently, our group reported that Li^+ ion hopping conduction occurs in highly concentrated Li salt/sulfolane electrolytes.[10] Similar Li^+ transport was also observed for the highly concentrated LiFSA/keto ester electrolytes.[11] It was found that the solvent molecules, with two coordinating sites, bridge different Li^+ ions, resulting in the formation of the solvent-bridged network structures of Li^+−solvent−Li^+ in these highly concentrated electrolytes. Therefore, highly concentrated electrolytes with certain solvents having multiple coordinating sites are anticipated to exhibit Li^+ ion hopping conduction. Here, we undertook a study of the phase behavior, coordination structures and diffusional behavior of binary mixtures of LiFSA and short-chain alkyl dinitriles. We then further

assessed the thermal and electrochemical properties of the mixtures, and investigated the potential for application of one of the promising electrolytes for electrochemical electrode reactions in Li-ion battery systems.

EXPERIMENTAL SECTION

Purified LiFSA and SN were purchased from Kishida Chemical and used as received. GN and ADN were purchased from Tokyo Chemical Industry Co. and dried over molecular sieves (3A) for several days before use. AN (super dehydrated) was purchased from Wako Pure Chemical Industries and used as received. LiTFSA was kindly supplied by Solvay Japan. Li salt and dinitrile solvents were mixed in the appropriate molar ratios and stirred at 60 °C for 24 h in an Ar-filled glovebox. Some of the mixtures having higher melting points were heated to 100 °C to obtain homogeneous samples. The thermal properties of the binary mixtures of Li salt and dinitrile were evaluated using a differential scanning calorimetry (DSC7020, Hitachi High-Tech Science). The samples for DSC were sealed in aluminum pans in an Ar-filled glovebox. The sample pans were first heated to 100 °C to erase thermal hysteresis, followed by cooling to −150 °C and finally heating to 100 °C at a rate of 5 °C min^{-1}. The thermograms in the final heating process were analyzed. The melting point (T_m) of a sample was estimated from the maximum point of the endothermic peak, and the glass transition temperature (T_g) was estimated from the onset of the change in heat capacity, respectively. Thermogravimetric measurement was performed on a TG/TDA 6200 (Seiko) to estimate the thermal stability of the studied mixtures. For assessing temperature dependent stability, the samples were heated from room temperature to 550 °C at a heating rate of 10 °C min^{-1}.

Single crystal X-ray crystallography was performed on a Rigaku XtaLAB PRO diffractometer using

monochromatic Mo Kα radiation (λ= 0.71073 Å). The single crystals of the crystalline solvates were coated with vacuum grease to prevent contact with air and mounted on a glass pin. The diffraction was measured at low temperature using a steady flow of −50 ℃ nitrogen gas. An empirical absorption correction was applied to the obtained data using multiscan averaging of symmetry equivalent data using spherical harmonics, implemented in the SCALES3 ABSPACK scaling algorithm (CrysAlisPro 1.171.39.46e, Rigaku Oxford Diffraction, 2018). The crystallographic structure was solved by the direct method using SHELXT and all non-hydrogen atoms were refined anisotropically by the full-matrix least-squares method using SHELXL-2018/3.[12,13] Raman spectra were measured using a Raman spectrometer with a 785 nm laser (NRS-4100, JACSO) and the instrument was calibrated using a polypropylene (for spectra in the range 680-790 cm^{-1}) or acetonitrile/toluene mixture (for spectra in the range 2220-2320 cm^{-1}) standard before the measurements. The spectroscopic resolution was 4.6 cm^{-1}. The samples were sealed in a capillary tube, and their temperature was controlled using a Peltier microscope stage (TS62, INSTEC) with a temperature controller (mk1000, INSTEC).

The ionic conductivity (σ) of samples was determined by the complex impedance method using an impedance analyzer (VMP, Biologic) in the frequency range of 500 kHz-1 Hz with a sinusoidal alternating voltage amplitude of 10 mV root-mean-square (rms). A two platinized platinum electrodes cell (CG-511B, TOA Electronics) was utilized for the conductivity measurements, and the cell constant was determined using a 0.01 M KCl aqueous solution at 25 ℃ prior to the measurements. The density and viscosity were determined using a viscometer (SVM 3000, Anton Paar), and the Li salt concentration (c_{Li}) was determined from the density value and the molecular weight of the electrolytes. Pulsed field gradient (PFG) NMR measurements were carried out to determine the self-diffusion coefficients of the Li^+, FSA^-, and dinitrile in the electrolytes using a bipolar pulse-pair longitudinal eddy current delay

(BPP-LED) pulse sequence with sinusoidal PFG.[14,15] A JEOL-ECX 400 NMR spectrometer with a 9.4 T narrow-bore superconducting magnet equipped with a pulsed-field gradient probe and current amplifier was used for the measurements of the solvents (^{1}H, 399.7 MHz), FSA anions (^{19}F, 376.1 MHz), and lithium cations (^{7}Li, 155.3 MHz). The diffusion echo signal attenuation, E, is related to the experimental parameters by the Stejskal equation with a sinusoidal pulsed-field gradient:

$$\ln(E) = \ln(S/S_{\delta=0}) = \frac{-4\gamma^2 g^2 D\delta^2(\Delta - \frac{2\delta}{3\pi} - \frac{\tau_g}{2})}{\pi^2} \qquad \text{(Eq.1)}$$

where S is the spin-echo signal intensity, δ is the duration of the field gradient with magnitude g, γ is the gyromagnetic ratio, τ_g is the time interval between the bipolar gradients, and Δ is the diffusion time. The values of Δ, δ, τ_g, and g were set to 20~100 ms, 3~5 ms, 1.0 ms, and 0.01~13 T m^{-1} depending on the electrolyte. The sample was inserted into an NMR microtube (BMS-005J Shigemi) to a height of 3 mm to exclude convection, and the measurements were performed at 30 or 60 °C.

Cyclic voltammetry was performed with a three-electrode cell using an electrochemical analyzer (VMP3, Biologic). Cu disk electrode (3 mm in diameter) was used as the working electrode and a Pt wire was used as the counter electrode. The reference electrode was Li metal soaked in a 1 mol dm^{-3} Li[TFSA]/propylene carbonate solution, confined in a glass tube with a Pt liquid junction. For the estimation of limiting current density in the electrolytes, symmetrical [Li metal | electrolyte | Li metal] cells were fabricated in an Ar-filled glove box. Li metal foil was purchased from Honjo Metal and cut into a disk shape (16 mm in diameter). A glass fiber filter (GA-55, Advantec, 200 μm thickness) was inserted between the two Li metal electrodes as separator. The Li metal electrodes and the electrolyte (140 μl) were encapsulated into a 2032-type coin cell. Battery tests of the Li[FSA]/SN=1/0.8 electrolyte were carried out in half-cells with Li metal and either $LiNi_{1/3}Mn_{1/3}Co_{1/3}O_2$ or graphite electrodes. The $LiNi_{1/3}Mn_{1/3}Co_{1/3}O_2$ electrode was composed of 80 wt% $LiNi_{1/3}Mn_{1/3}Co_{1/3}O_2$ powder (AGC Seimi

Chemical), 10 wt% acetylene black (Denki Kagaku Kogyo), and 10 wt% poly(vinylidene fluoride) (Kureha Chemical). These materials were mixed together and thoroughly agitated in *N*-methylpyrrolidone (Kanto Chemical) with a homogenizer. The slurry was coated onto Al foil with a doctor blade apparatus to prepare a composite sheet and dried overnight at 80 ℃. The composite sheet was then cut into a disk (16 mm diameter) and compressed at 50 MPa, followed by drying under vacuum at 120 ℃ for 12 h. The thickness of the composite layer on Al foil was 20 μm, and the loading of $LiNi_{1/3}Mn_{1/3}Co_{1/3}O_2$ was 4.0-4.3 mg cm^{-2}. The graphite electrode was composed of 90 wt% artificial graphite powder (Hitachi Chemical), 3 wt% acetylene black, and 7 wt% poly(vinylidene fluoride). These materials were mixed together and thoroughly agitated in *N*-methylpyrrolidone with a homogenizer. The slurry was coated onto Cu foil with a doctor blade apparatus to prepare a composite sheet and dried overnight at 80 ℃. The composite sheet was then cut into a disk (16 mm diameter) and compressed at 50 MPa followed by drying in a vacuum at 120 ℃ for 12 h. The thickness of the composite layer on Cu foil was 40 μm, and the loading of graphite was 3.6 mg cm^{-2}. A $LiNi_{1/3}Mn_{1/3}Co_{1/3}O_2$ half-cell and a graphite half-cell were fabricated with the [LiFSA]/[SN] = 1/0.8 electrolyte. A Li metal counter electrode, the electrolyte of [LiFSA]/[SN] = 1/0.8, and a composite sheet electrode were encapsulated into a 2032 type coin cell. A glass fiber filter (GA-55, Advantec) was used as the separator between the counter electrode and the composite electrode. The cells were kept at 60 °C for 12 h prior to electrochemical measurements to ensure the penetration of electrolytes into the composite sheet electrodes. Galvanostatic charge–discharge tests were carried out using an automatic charge/discharge instrument (HJ1001SD, Hokuto Denko) in the voltage range of 2.5–4.2 V for the $LiNi_{1/3}Mn_{1/3}Co_{1/3}O_2$ half-cell and 0.001–2.0 V for the graphite half-cell at 30 ℃.

RESULTS AND DISCUSSION

Solvation Structure. DSC thermograms of LiFSA/SN binary mixtures are shown in **Figure 2**. The melting point (T_m) of neat SN is 57 °C and the T_m of the mixture decreases with increasing molar ratio of [LiFSA]/[SN] up to 1/10. Aside for the peak due to the melting process, several endothermic peaks are observed due to solid-solid phase transitions. The endothermic peak at −38 °C is assigned to the crystal-plastic crystal phase transition of SN,[16] and the peaks between −38 °C and T_m are probably due to the phase transition from one plastic crystal to another plastic crystal. The origin of the thermal event observed at −70 °C for the mixtures of [LiFSA]/[SN] ≥ 1/4 is not clear at present. In the range 1/10 ≤ [LiFSA]/[SN] ≤ 1/2, T_m increases gradually as the molar ratio of LiFSA increases, suggesting that LiFSA and SN form a stable complex, i.e., a solvate LiFSA-$(SN)_2$ (T_m: 63.4 °C). At a molar ratio higher than [LiFSA]/[SN] = 1/1, the mixture becomes a glass forming liquid, and the [LiFSA]/[SN] = 1/0.8 mixture maintains a liquid state at room temperature.

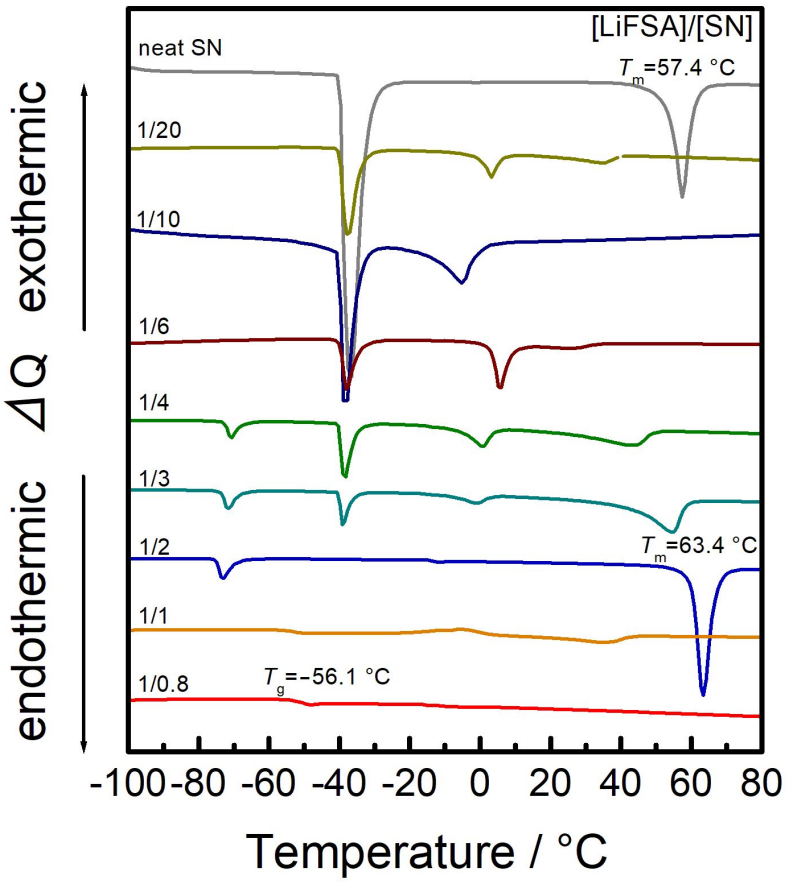

Figure 2. DSC thermograms of binary mixtures of LiFSA and SN (molar ratio of [LiFSA]/[SN] = 1 /*n*).

The crystal structure of the LiFSA-$(SN)_2$ solvate was investigated using X-ray crystallographic analysis. A single crystal of the LiFSA-$(SN)_2$ solvate was successfully grown in the binary mixtures of LiFSA/SN = 1/6 at room temperature. Due to the disorder of the anion (FSA^-) in the LiFSA-$(SN)_2$ crystal, the refinement of the crystal structure is not optimal (poor R_1 and wR_2 values, as shown in **Table S1**). Although the precision of the structural analysis is lacking, it still provides useful information on the coordination environment of Li^+. As shown in **Figure 3**, the coordination number of Li^+ is 4 in the LiFSA-$(SN)_2$ crystal. All the SN molecules adopt the *trans* conformation and bridge different Li^+ ions, forming a network structure (Li^+−SN−Li^+). As can be seen in **Figure 3**, FSA^- anions do not participate in the coordination of Li^+ ions, and Li^+ and FSA^- form solvent separated ion pairs (SSIPs) in the crystal. For

comparison, the solvate structure of LiTFSA-$(SN)_n$ was also investigated. In the case of LiTFSA/SN mixtures, a stable solvate is formed at a molar ratio of [LiTFSA]/[SN] = 1/1.5 (T_m: 59.0 °C) (**Figure S1**). In the LiTFSA-$(SN)_{1.5}$ crystal (**Figure S2 and Table S2**), the SN molecules adopt a *trans* conformation and bridge different Li^+ ions as was case for the LiFSA-$(SN)_2$ crystal. Here we note that Henderson et al. reported the crystal structures of $LiF_2BC_2O_4$-$(SN)_1$ and $LiBF_4$-$(SN)_1$ solvates.[17,18] The SN molecules have *cis* and *gauche* conformations in $LiF_2BC_2O_4$-$(SN)_1$ and $LiBF_4$-$(SN)_1$, respectively, and, again, Li^+ ions are bridged by SN in each crystal. The phase behaviors of LiFSA/glutaronitrile (GN) and LiFSA/adiponitrile (ADN) systems were also studied (**Figure S3 and Figure S4**). DSC thermograms suggested that LiFSA and these dinitrile solvents form stable solvates at the 1/2 molar ratio, irrespective of the increasing intramolecular distance between the two cyano groups. The melting point of the LiFSA-$(dinitrile)_2$ solvate increases with the molecular weight of dinitrile as shown in **Table 1**. Although the refinement of the structure is not optimal, the single crystal X-ray crystallography suggested that Li^+ ions are bridged by ADN molecules and the FSA^- anions do not coordinate to the Li^+ ion in the LiFSA-$(ADN)_2$ solvate crystal structure (**Figure S5 and Table S3**). Unfortunately, the crystal structure of the LiFSA-$(GN)_2$ solvate could not be determined because of the low crystallinity.

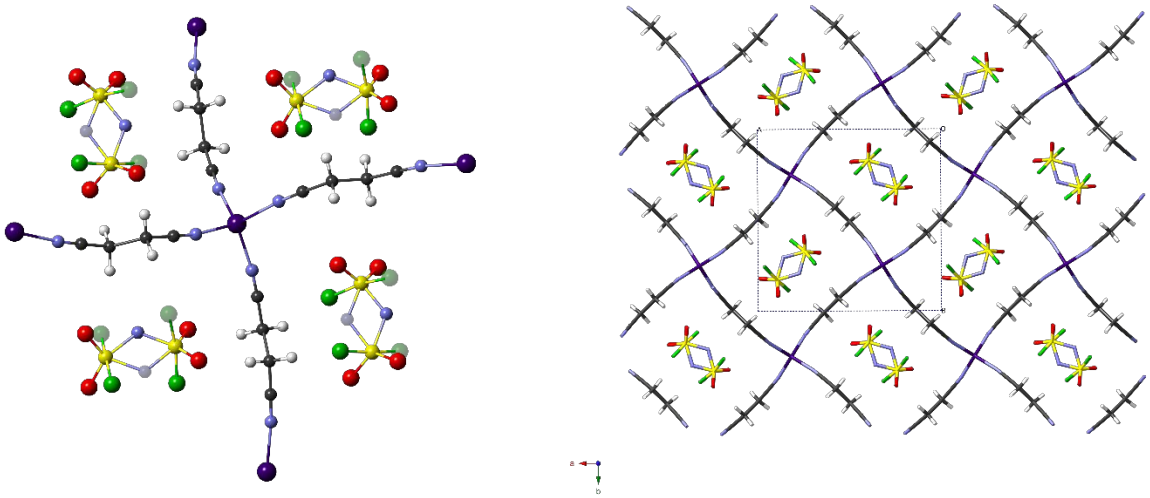

Figure 3. Ball and stick model (left) and packing diagram (right) for the LiFSA-$(SN)_2$ crystal. Note that

disordered atoms on FSA anion (N, and F) are shown in the figure. White, H; purple, Li; red, O; black, C; yellow, S; green, F; blue, N. Due to the poor R_1 and wR_2 values, a corresponding cif file has not been deposited in the CCDC.

Table 1. The melting points (T_m) and glass transition temperatures (T_g) of [LiFSA]/[dinitrile]=1/0.8 and 1/2 (dinitrile: SN, GN, ADN).

[LiFSA]/[dinitrile]	T_g / °C	T_m / °C
[LiFSA]/[SN] = 1/2	-	63.4
[LiFSA]/[GN] = 1/2	-	89.3
[LiFSA]/[ADN] = 1/2	-	90.9
[LiFSA]/[SN] = 1/0.8	−56.1	-
[LiFSA]/[GN] = 1/0.8	−61.3	39.6
[LiFSA]/[ADN] = 1/0.8	−63.1	47.9

The Raman spectra for the liquid state mixtures of LiFSA/SN in the range of 2220-2320 cm^{-1} are shown in **Figure 4a**. The neat SN shows a peak at 2253 cm^{-1} assigned to the C≡N stretching vibration,[19] and this peak shifts to a higher wavenumber by mixing LiFSA and SN in a 1:10 ratio. In the case of the LiFSA-excess mixture, i.e. [LiFSA]/[SN] ≥ 1/2, the peak splits into two, centered at 2278 cm^{-1} and 2253 cm^{-1}, and the intensity of the higher wavenumber peak increases with increasing molar ratio of LiFSA. For comparison, the Raman spectrum of the solid state solvate of LiFSA-$(SN)_2$ is also shown in **Figure 4b**. The solid state LiFSA-$(SN)_2$ solvate showed a sharp peak at 2278 cm^{-1}. Taking into account the crystal structure of LiFSA-$(SN)_2$ solvate, the vibrational mode observed at 2278 cm^{-1} is assignable to the cyano group coordinated to the Li^+ ion. Upon melting of the LiFSA-$(SN)_2$ crystal, the peak corresponding to a free cyano group, which is not bound to Li^+, appeared at 2254 cm^{-1}, suggesting that a certain proportion of the cyano groups are free (i.e. non-coordinating) following the solid to liquid phase transition. Consequently, the solvent-bridged structure is partially disrupted by the transition, and thus there are SN molecules for which only one of the two cyano groups are bound to Li^+ and indeed for

which both cyano groups are non-coordinating.

In the spectrum of [LiFSA]/[SN]=1/0.8 (**Figure 4a**), the peak area of the bound cyano group (2278 cm^{-1}) is much larger than that of free one (2253 cm^{-1}). The Raman spectrum of the liquid of [LiFSA]/[SN]=1/0.8 was deconvoluted into two peaks corresponding to the bound and free cyano groups (**Figure S6**). According to the previous reports, the Raman scattering coefficients for the bound and free cyano groups are almost identical for acetonitrile.[20] Assuming that the Raman scattering coefficient for the C≡N stretching band is the same for the bound and free cyano groups in the [LiFSA]/[SN]=1/0.8 mixture, the fraction of free cyano *group* was evaluated to be 5.5% (**Figure S6 and Table S4**). This suggests that a large fraction of SN molecules bridge Li^+ ions, in other words, the solvent-bridged structure (Li^+−SN−Li^+) is maintained even in the liquid state. The amount of free SN *molecules*, i.e. whose two cyano groups are both free, was estimated to be only 0.3 % (= 0.055^2×100 %) in the liquid. It is also noteworthy that decreasing the amount of free SN in the mixture is effective in lowering the vapor pressure of SN. The results of thermogravimetric analysis (**Figure S7**) demonstrated that the 5% mass loss temperatures for neat SN (without LiFSA) and [LiFSA]/[SN]=1/0.8 are 153 and 200 °C, respectively. Accordingly, the highly concentrated LiFSA/SN electrolyte possesses a relatively high thermal stability.

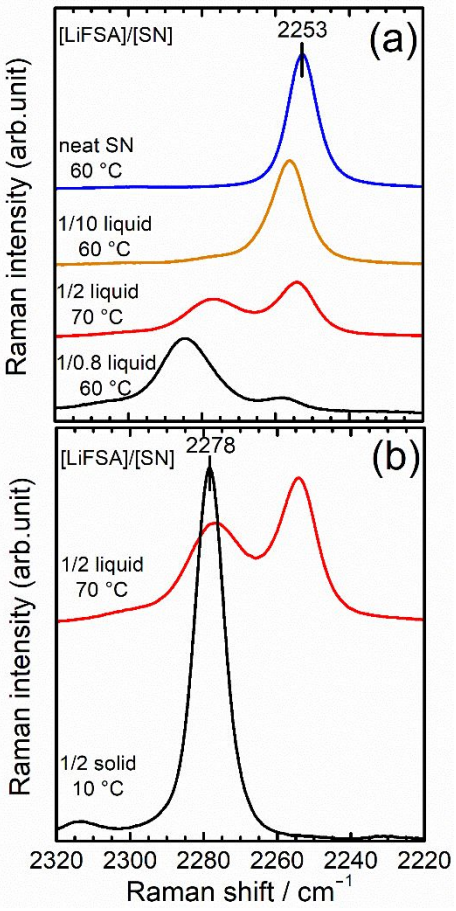

Figure 4. Raman spectra in the range corresponding to the C≡N stretching vibration of the cyano group of SN in the LiFSA/SN binary mixtures at various molar ratios ([LiFSA]/[SN] = 1 /*n*) (a) and the LiFSA-$(SN)_2$ solvate (b).

Figure 5 shows the Raman spectra of the S-N-S stretching vibration of the FSA^- anion.[11,21,22] The peak is observed at 729 cm^{-1} for the solid state solvate of LiFSA-$(SN)_2$. As revealed by the crystallography, FSA^- anion is not bound to Li^+ and exists as a SSIP-type anion in the solid (**Figure 5a**). Upon melting, the peak of FSA^- shifts to higher wavenumber (739 cm^{-1}). According to the literature, the peak shift to higher wavenumber is due to the formation of a contact ion pair (CIP) of LiFSA.[21] The Raman spectra corresponding to the C≡N stretching vibration of the cyano group suggested that a certain proportion of cyano group was disconnected from the Li^+ ion (i.e. became non-coordinating) upon melting (**Figure 4**). Thus, the Raman spectral change observed for the anion in LiFSA-$(SN)_2$ upon the solid to liquid phase

transition (**Figure 5a**) suggested that subsequently in the liquid, the FSA^- anion is bound to Li^+ to satisfy its coordination number (*vide infra*). **Figure 5b** shows the Raman spectra for LiFSA/SN mixed in various molar ratios. In the case of [LiFSA]/[SN] = 1/10, the Raman band of the S-N-S stretching vibration was observed at 730 cm^{-1}, which is close to that of the crystalline solvate of LiFSA-$(SN)_2$, indicating that the FSA^- exists in the liquid as a free or SSIP anion. In other words, the Li^+ is mainly solvated by SN molecules in the liquid of [LiFSA]/[SN] = 1/10, and FSA^- anion scarcely exists in the first solvation shell of Li^+. The peak of FSA^- shifts to a higher wavenumber with increasing LiFSA molar ratio, and the corresponding S-N-S stretch Raman peak center for [LiFSA]/[SN] = 1/0.8 is as high as 753 cm^{-1}. The relatively large Raman shift (~750 cm^{-1}) suggests the formation of ionic aggregates (AGGs), in which FSA^- anions bind to multiple Li^+ ions, i.e., the formation of an anion-bridged structure of $Li^+{-}FSA^-{-}Li^+$.[11,21] The coordination number of Li^+ is commonly in the range of 4-5 in liquids.[23–25] In the [LiFSA]/[SN] = 1/0.8 mixture, the ratio of [Li^+]/[cyano group] is 1/1.6; therefore, the coordination number of Li^+ cannot be fulfilled solely by cyano groups, and the FSA^- anions should be involved in the coordination. The solvation structures of GN- and ADN-based liquids were also investigated. At a molar ratio of [LiFSA]/[dinitrile] = 1/0.8, the S-N-S stretch Raman peak of the FSA^- anion appeared at ~750 cm^{-1} (**Figure S8**), suggesting that AGGs are also formed in these solvent-deficient liquids.

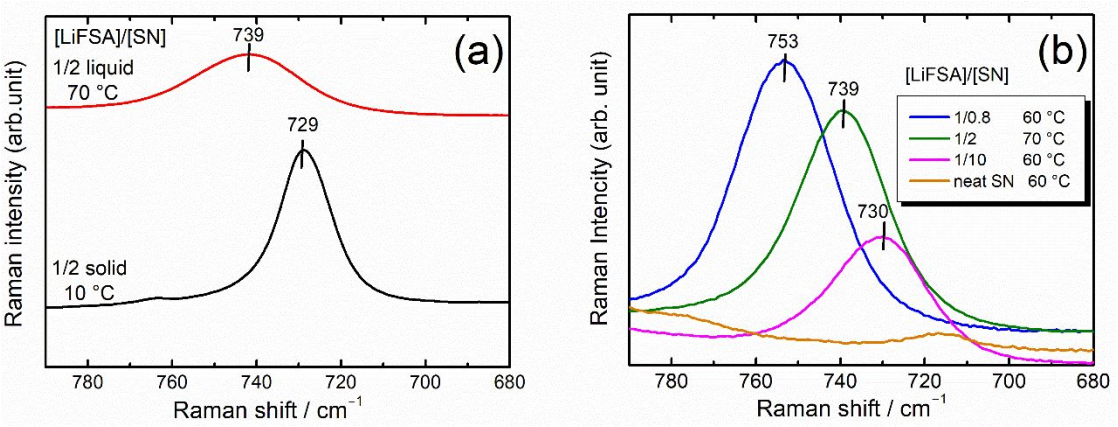

Figure 5. Raman spectra in the range corresponding to the S-N-S stretching vibration of FSA^- in the LiFSA-$(SN)_2$ solvate (a), and LiFSA/SN binary mixtures with various molar ratios ([LiFSA]/SN = 1/n) (b).

Transport Properties. The ionic conductivity (σ) and viscosity (η) of LiFSA/SN mixtures was measured. The viscosity of LiFSA/SN electrolyte increases with increasing Li salt concentration. The mixture of [LiFSA]/[SN] = 1/0.8 is extremely viscous (η ~3000 mPa s) at room temperature, and its ionic conductivity is as low as 0.26 mS cm^{-1} (**Table 2**). However, the ionic conductivity increases with increasing temperature and becomes higher than 1 mS cm^{-1} at 60 °C. (**Figure S9**). The molar conductivity (Λ) of selected LiFSA/SN mixtures was plotted against 1/η (Walden plot) as shown in **Figure S10**. Λ for [LiFSA]/[SN] = 1/0.8 becomes higher than the KCl ideal line. The KCl ideal line is the Walden line for the 1 mol dm^{-3} KCl aqueous solution, in which the KCl is assumed to be completely dissociated. The Λ value, exceeding that of KCl, for [LiFSA]/[SN] = 1/0.8 suggests that the ionic conductivity tends to be decoupled from viscosity.[26]

To further elucidate the transport properties in the liquids, the self-diffusion coefficients of Li^+ (D_{Li}), $[FSA]^-$ (D_{FSA}), and SN (D_{SN}) were measured using PFG-NMR. The plots of signal attenuation $\ln(S/S_{\delta=0})$ versus $k = -4\gamma^2 g^2 \delta^2 (\Delta - 2\delta/3\pi - \tau_g/2)/\pi^2$ for the SN (^{1}H), FSA (^{19}F), and Li^+ (^{7}Li) PFG-NMR echo signals of LiFSA/SN mixtures are shown in **Figure S11**. The self-diffusion coefficients are determined

from the slope of the plots (Eq.1), where a steeper slope suggests faster diffusion. The self-diffusion coefficients of the species are summarized in **Table 2**. With increasing LiFSA concentration, the diffusion coefficients of the species in the liquid become lower due to the increase in viscosity. The order of diffusion coefficients in the solvent excess mixtures ([LiFSA]/[SN] = 1/6 and 1/10) is $D_{SN} > D_{FSA} > D_{Li}$. According to the Stokes-Einstein equation, the diffusivity is proportional to the reciprocal of hydrodynamic radius. Owing to solvation in liquids, the hydrodynamic radius of Li^+ becomes larger than the ionic radius observed for Li^+ in typical crystalline solids. In the solvent excess liquids, the Li^+ ion diffuses as a solvated ion ($[Li(SN)_n]^+$), *viz*., vehicular-type ion conduction mechanism, and the diffusion coefficient of Li^+ becomes lower than that of the solvent (SN). However, the NMR measurement could not distinguish the uncoordinated- and coordinated-SN molecules. This is because the Li^+ ion exchanges ligands (solvent molecules) in the first solvation shell dynamically on a shorter time scale compared to the NMR time scale.[27,28]

In sharp contrast to the solvent excess mixtures, in the highly concentrated [LiFSA]/[SN] = 1/0.8 electrolyte, the diffusion coefficient of Li^+ is larger than that of solvent and anion, $D_{Li} > D_{SN} \approx D_{FSA}$ (**Figure S11c** and **Table 2**). Similar results were also obtained for [LiFSA]/[GN] = 1/0.8 and [LiFSA]/[ADN] = 1/0.8 (**Figure S12** and **Table 3**). These indicate that the Li^+ ion transport mechanism in the highly concentrated dinitrile-based liquid electrolytes is different from that of solvent excess liquids. Previously, we reported Li^+ ion hopping conduction in other electrolyte solutions with high Li salt concentrations.[10,11] The faster diffusion of Li^+ compared to the solvent and anion suggests that Li^+ exchanges the ligands (solvent and anion) and moves forward leaving behind the ligands. As revealed by the Raman spectroscopy, in the liquids comprised of LiFSA/dinitrile, each dinitrile molecule bridges two different Li^+ ions and forms solvent-bridged structures when the molar ratio of LiFSA is higher. In

addition, the FSA^- anion also coordinates to two or more Li^+ ions, resulting in the formation of anion-bridged structures. In the aggregates (AGGs) composed of Li^+ ions and ligands (solvent and anion), each ligand is interacting with multiple Li^+ ions. Moreover, AGGs are adjacent to each other in the highly concentrated electrolytes. This would restrict the translational motions of ligands. Of course, the liquid structure changes dynamically; however, the solvent- and/or anion-bridged structures are akin to the continuous framework structure for ion conduction in the inorganic solid electrolytes.[29] Consequently, one can presume that Li^+ ion hopping conduction occurs through ligand-exchange in the AGG (solvent- and/or anion-bridged structures). We note here the crucial role of the solvent-bridged structure for the Li^+ ion hopping conduction. The transport properties of [LiFSA]/[AN] = 1/1.6, in which the ratio of $[Li^+]$/[cyano group] is identical to that of [LiFSA]/[SN] = 1/0.8, were also investigated. In the liquid of [LiFSA]/[AN] = 1/1.6, the Li^+ ions are bridged by FSA^- anions and AGGs are formed.[21] The self-diffusion coefficients of species in the [LiFSA]/[AN] = 1/1.6 electrolyte were measured (**Figure S13**), and the obtained values are displayed in **Table 4**. Regardless of the formations of AGGs in the liquid, Li^+ ion diffuses slower than AN. This is probably because AN is a simple monodentate-type ligand interacting with a single Li^+ ion, and the solvent-bridged structure cannot be formed in the liquid. In addition, the AN is a compact solvent, and the viscosity of the [LiFSA]/[AN] = 1/1.6 is relatively low compared to that of [LiFSA]/[SN] = 1/0.8. These may cause the faster diffusion of AN than Li^+ in the liquid. However, the diffusion coefficient of Li^+ is higher than that of FSA^- in the liquid with a composition of [LiFSA]/[AN] = 1/1.6, indicating that the Li^+ ion exchanges the anions and the anion-exchange conduction mechanism emerges in the anion-bridged structure.

Table 2. Viscosity (η), density (ρ), concentration of LiFSA (c), ionic conductivity (σ), and self-diffusion coefficients of electrolytes of LiFSA/SN at 30 °C.

molar ratio [LiFSA]/[SN]	η / mPa s	ρ / g cm^{-3}	c / mol dm^{-3}	σ / mS cm^{-1}	D_{Li} / 10^{-7} cm^2 s^{-1}	D_{FSA} / 10^{-7} cm^2 s^{-1}	D_{SN} / 10^{-7} cm^2 s^{-1}
1/0.8	3142	1.627	6.48	0.26	0.11	0.06	0.07
1/6	20	1.186	1.78	5.91	5.04	5.47	5.78
1/10	13	1.121	1.13	5.83	9.8	10.9	12.4

Table 3. Ionic conductivity (σ), and self-diffusion coefficients of electrolytes of [LiFSA]/[dinitrile] = 1/0.8 at 60 °C.

dinitrile	σ / mS cm^{-1}	D_{Li} / 10^{-7} cm^2 s^{-1}	D_{FSA} / 10^{-7} cm^2 s^{-1}	$D_{dinitrile}$ / 10^{-7} cm^2 s^{-1}
SN	1.63	0.71	0.48	0.47
GN	1.75	0.80	0.58	0.49
ADN	1.39	0.72	0.58	0.45

Table 4. Viscosity (η), density (ρ), concentration of LiFSA (c), ionic conductivity (σ), and self-diffusion coefficients of electrolytes of [LiFSA]/[AN] = 1/1.6 electrolyte at 30 °C.

molar ratio [LiFSA]/[AN]	η / mPa s	ρ / g cm^{-3}	c / mol dm^{-3}	σ / mS cm^{-1}	D_{Li} / 10^{-7} cm^2 s^{-1}	D_{FSA} / 10^{-7} cm^2 s^{-1}	D_{AN} / 10^{-7} cm^2 s^{-1}
1/1.6	90	1.458	5.77	3.50	1.96	1.67	2.91

Electrochemical Properties. The electrochemical properties of highly concentrated SN-based electrolyte were studied. At first, the reductive stabilities of LiFSA/SN solutions were evaluated by cyclic voltammetry using a three-electrode cell. The cyclic voltammogram of [LiFSA]/[SN] = 1/10 indicates the irreversible reductive decomposition of SN occurs at electrode potentials lower than 0 V (vs. Li/Li$^+$) (**Figure S14a**). On the other hand, in the [LiFSA]/[SN] = 1/0.8 electrolyte, the reductive decomposition of SN is suppressed, and reversible Li metal deposition/stripping is possible (**Figure S14b**). This suppression of reductive decomposition of SN may be due to the passivation layer formation on the electrode derived from the FSA$^-$ anion.[2,30] Yamada et al. reported the reversible Li deposition/stripping in highly concentrated LiTFSA/AN solution. According to their first principle calculations, the lowest unoccupied molecular orbital (LUMO) energy level of an amide-type anion is lowered by the complexation with Li$^+$, and the reductive decomposition of the anion occurs prior to the

decomposition of the nitrile solvents. They claimed that the decomposition products of the amide-type anion form a passivation layer on the electrode and suppress the decomposition of the solvents. Here, Raman spectra of the [LiFSA]/[SN] = 1/0.8 mixture suggested that a significant amount of FSA^- anion is involved in the coordination of Li^+. Therefore, it is inferred that a passivation layer derived from FSA^- anion is formed on the electrode surface in the [LiFSA]/[SN] = 1/0.8 electrolyte, resulting in the suppression of the reductive decomposition of SN. We note here that the stability of the passivation layer depends of the anion species. Nilsson et al. reported the instability of the passivation layer derived from $TFSA^-$ anion during the charge and discharge reactions in lithium ion batteries with highly concentrated LiTFSA/AN electrolytes.[3] However, the FSA^- derived passivation layer may have better stability compared to that derived from $TFSA^-$ anion. Indeed, several groups reported the high reversibility of the Li metal deposition/dissolution in electrolytes containing LiFSA salt.[30–33]

To examine the effects of transport properties on the limiting current density in highly concentrated LiFSA/SN electrolytes, chronoamperometry (CA) was conducted using a symmetric [Li metal | electrolyte | Li metal] cell. During the CA measurements, Li deposition and dissolution occur at the cathode and the anode, respectively. **Figure 6a** shows the current responses of the cell with the [LiFSA]/[SN] = 1/0.8 electrolyte at various applied voltages. The faradaic current is observed from the moment the voltage is applied, and the current hardly decays with time when the voltage is lower than 500 mV. At a voltage higher than 600 mV, the current increases slightly at the initial stage of the electrolysis. This is probably due to the roughening of the Li metal surface during the deposition and dissolution. At higher than 700 mV, we could not obtain reproducible data because the internal short-circuit occurred due to the dendritic deposition of Li at the cathode. The time-independent current observed at lower than 500 mV (**Figure 6a**) indicates that the concentration polarization of LiFSA in the

electrolyte was not so remarkable at current density lower than 4.5 mA cm^{-2} despite the electrochemical reactions at the cathode and the anode. This behavior is similar to that of a symmetric [Li| electrolyte |Li] cell with a highly concentrated $LiBF_4$/sulfolane electrolyte.[10] We reported that the Li^+ hopping conduction suppresses the concentration polarization.[10] Owing to the hopping conduction, the transference number of Li^+, t_{Li+}, in the electrolyte becomes higher. The t_{Li+} estimated from the self-diffusion coefficients of Li^+ and FSA anion ($t_{Li+} = D_{Li} /(D_{anion} + D_{Li})$) in the [LiFSA]/[SN] = 1/0.8 electrolyte is as high as 0.62 while the t_{Li+} in the solvent-excess electrolytes ([LiFSA]/[SN] = 1/6 and 1/10) is 0.47. The t_{Li+} in the [LiFSA]/[SN] = 1/0.8 electrolyte was also evaluated by an electrochemical method (Electronic Supplementary Information),[34] and the estimated value is as high as 0.74 (**Figure S15** and **Table S5**). The t_{Li+} value determined by the electrochemical method (t_{Li+}(EC)) is slightly higher than that estimated from self-diffusion coefficients (t_{Li+}(NMR)). Actually, both the t_{Li+}(NMR) and t_{Li+}(EC) were estimated based on the assumption that LiFSA was completely dissociated into Li^+ cation and FSA^- anion that migrated independently, and the association of the Li^+ and FSA^- in the liquid was not considered. However, ion pairs and ionic aggregates are formed in the highly concentrated electrolytes (*vide supra*). This might cause the difference in the values of t_{Li+}(NMR) and t_{Li+}(EC). For more rigorous determination of t_{Li+}, further experimental data are needed, and concentrated electrolyte theory taking into account the formations of ion pairs and ionic aggregates should be applied.[35-39] In any case, the higher transference number is effective in suppressing the concentration polarization in the electrolyte.[40] As shown in **Figure 6a**, the faradaic current increases with applied voltage. The steady-state current density at 300 s is plotted against the applied voltage (**Figure 6b**), and the observed current at 700 mV is relatively high, reaching 7.0 mA cm^{-2}. Note that the diffusion-limiting current densities in 2.75 mol dm^{-3} LiTFSA/tetraglyme (σ = 1.6 mS cm^{-1}) and 1 mol dm^{-3} $LiClO_4$/propylene carbonate (σ =

6.4 mS cm^{-1}) are reported to be 1.1 and 9.2 mA cm^{-2}, respectively.[41] The [LiFSA]/[SN] = 1/0.8 electrolyte exhibits a relatively high Li^+ transport ability (≥ 7.0 mA cm^{-2}) thanks to the Li^+ hopping conduction and a high Li^+ transference number, although its ionic conductivity is as low as 0.26 mS cm^{-1}.

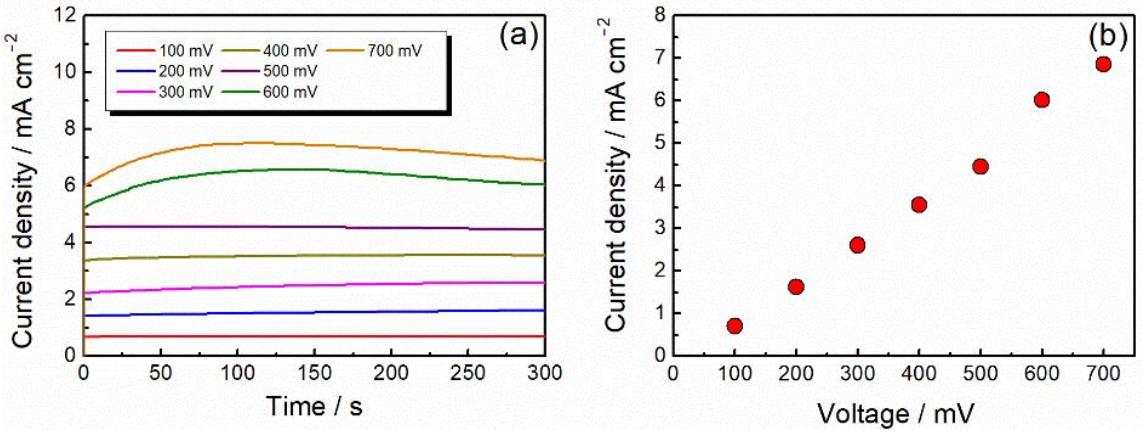

Figure 6. Chronoamperograms for symmetric [Li | [LiFSA]/[SN] = 1/0.8 with glass fiber filter separator (GA-55 (200 μm)) | Li] cell measured at various applied voltages at 30 °C.

The [LiFSA]/[SN] = 1/0.8 electrolyte was tested using practical electrodes for Li-ion batteries (LIBs). The charge and discharge reactions of graphite, which is an anode material of LIBs, were examined in the [Li | [LiFSA]/[SN] = 1/0.8 | graphite] cell. **Figure 7a** shows the charge-discharge curves of the graphite electrode. During the charging, Li^+ ion intercalation into the layered structure of graphite occurs in the voltage range 0.3−0 V, and the deintercalation of Li^+ from the lithiated graphite proceeds during the discharging. Although the Coulombic efficiency of the first charge-discharge cycle was 85%, the graphite electrode showed an excellent reversible behavior in the subsequent cycles with Coulombic efficiency of 99%. The irreversible charging capacity observed in the voltage range 1.5−0.3 V during the 1st charging is attributed to the reductive decomposition of the electrolyte on the graphite electrode. The decomposition products might form a passivation layer on the graphite, which prevents the decomposition of the electrolyte in the subsequent cycles.[2] The discharge capacity of the graphite

electrode was ca. 360 mAh g^{-1}, which is close to the theoretical capacity 372 mAh g^{-1}. The electrochemical reaction of acetylene black, which was contained in the graphite composite electrode as a conductive additive, might also contribute to the charge and discharge capacities. However, the content of acetylene black in the electrode was only 3wt%, therefore it is assumed that the contribution of acetylene black to the capacity would be very small. The coulombic efficiency of the discharge/charge was higher than 99% after the 2nd cycle. We note that the graphite half-cell showed unstable charge-discharge behaviour upon further cycling (not shown) due to the internal short circuit caused by the dendritic growth of Li metal at the Li counter electrode. Achieving a reversible lithium metal electrode is also of interest as the electrochemical deposition and dissolution of Li metal correspond to the charge and discharge reactions at the negative electrodes of Li metal batteries, such as Li-sulfur and Li-air batteries. Further elucidation may be needed to understand the dendritic growth of Li metal in the highly concentrated electrolytes and will be reported in due course.

Next, the charge and discharge reactions of $LiNi_{1/3}Mn_{1/3}Co_{1/3}O_2$, which is a cathode material of LIBs, were examined in the [Li | [LiFSA]/[SN] = 1/0.8 | $LiNi_{1/3}Mn_{1/3}Co_{1/3}O_2$] cell. **Figure 7b** shows the galvanostatic charge-discharge curves of a [Li | [LiFSA]/[SN] = 1/0.8 | $LiNi_{1/3}Mn_{1/3}Co_{1/3}O_2$] cell measured at a current density of 65 μA cm^{-2}. The redox reactions of $LiNi_{1/3}Mn_{1/3}Co_{1/3}O_2$ occur in the voltage range 3.7−4.2 V. The deintercalation of Li^+ ion from the crystal structure of $LiNi_{1/3}Mn_{1/3}Co_{1/3}O_2$ occurs during the charging process, and reverse reaction (intercalation of Li^+) takes place during the course of discharge. The cell showed a discharge capacity of ca. 150 mAh g^{-1}, and the charge-discharge behavior is highly reversible with Coulombic efficiency of 98%, suggesting that irreversible side reactions do not occur significantly in the cell. We note here that the corrosion of Al current collector of the $LiNi_{1/3}Mn_{1/3}Co_{1/3}O_2$ electrode does not occur significantly during the charge-discharge in the

[LiFSA]/[SN] = 1/0.8 electrolyte. The chronoamperogram of Al foil measured in the [LiFSA]/[SN] = 1/0.8 electrolyte indicated that the corrosion current of Al is effectively suppressed even at a high voltage of 4.8 V (**Figure S16**). It is known that the Al corrosion occurs at electrode potential higher than 4 V vs. Li/Li^+ in an electrolyte containing the FSA^- anion.[42-44] The suppression of Al corrosion is attributed to the very low activity of free cyano group, leading to the suppression of the solubility of the $Al(FSA)_x$ complex produced by the corrosion reaction at the Al/electrolyte interface.[45] The $Al(FSA)_x$ might function as a passivation layer on the Al surface.

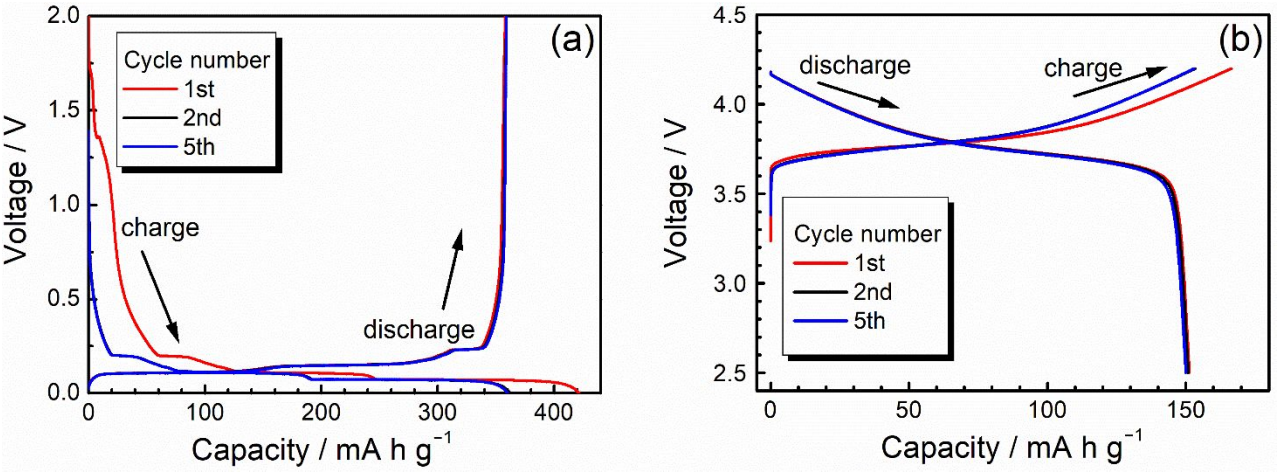

Figure 7. Galvanostatic charge-discharge curves of (a) [Li | [LiFSA]/[SN] = 1/0.8 | graphite] cell (current density : 68 μA cm^{-2}) and (b) [Li | [LiFSA]/[SN] = 1/0.8 | $LiNi_{1/3}Mn_{1/3}Co_{1/3}O_2$] cell (current density : 65 μA cm^{-2}) measured at 30 °C.

To investigate the effect of Li^+ ion hopping conduction on the rate capability of the [Li | [LiFSA]/[SN] = 1/0.8 | $LiNi_{1/3}Mn_{1/3}Co_{1/3}O_2$] cell, discharge measurements were carried out at various current densities (**Figure 8**). The discharge voltage decreases with increasing current density. The resistance for ion conduction in the electrolyte causes the ohmic drop. In addition, the overpotentials for the electrochemical reactions at Li metal and $LiNi_{1/3}Mn_{1/3}Co_{1/3}O_2$ electrodes increase with increasing current density. The discharge capacity decreased gradually with increasing current density, and the cell could not discharge at higher than 5.5 mA cm^{-2}. The decrease of the capacity was ascribed to the

limitation of Li^+ ion transport. During discharge, Li^+ ions are transported from Li metal to the $LiNi_{1/3}Mn_{1/3}Co_{1/3}O_2$ electrode in the electrolyte. As shown in **Figure 6**, the limiting current density in the electrolyte is higher than 7 mA cm^{-2} in the symmetric [Li||Li] cell. However, the $LiNi_{1/3}Mn_{1/3}Co_{1/3}O_2$ electrode is a porous composite electrode composed of $LiNi_{1/3}Mn_{1/3}Co_{1/3}O_2$ particles, acetylene black, and poly(vinylidene fluoride), and the thickness of the composite electrode is 20 μm. Therefore, the complicated conduction path for the Li^+ ion in the porous electrode might lower the limiting current density in the [Li | [LiFSA]/[SN] = 1/0.8 | $LiNi_{1/3}Mn_{1/3}Co_{1/3}O_2$] cell.

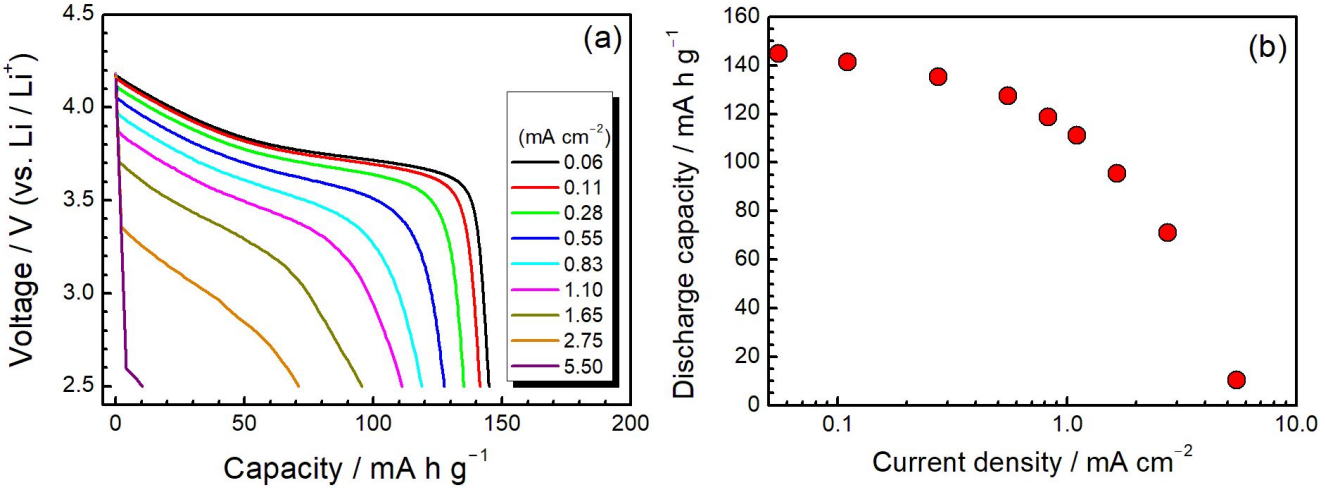

Figure 8. (a) Discharge curves [Li | [LiFSA]/[SN] = 1/0.8 | $LiNi_{1/3}Mn_{1/3}Co_{1/3}O_2$] cell measured at various current densities at 30 °C. (b) Discharge capacities of the cell. Prior to each discharge measurement, the cell was fully charged at a low current density of 55 μA cm^{-2}.

CONCLUSIONS

Phase behaviors of the LiFSA/dinitriles (SN, GN, and ADN) suggested that LiFSA and dinitriles form stable solvates in the molar ratio of 1:2, irrespective of the intramolecular distance between the two cyano groups. The two cyano groups of each dinitrile molecule coordinate to different Li ions and form solvent-bridged structures of Li^+−dinitrile−Li^+ in the solid solvates of LiFSA-$(dinitrile)_2$. At the ratio of [LiFSA]/[dinitrile] > 1, the binary mixtures become glass forming liquids, and the [LiFSA]/[SN] = 1/0.8 maintains a liquid state at room temperature. In the liquid state mixtures of [LiFSA]/[dinitrile] >1, the

solvent-bridged structure of Li^+−dinitrile−Li^+ and the anion bridged structure of Li^+−FSA^-−Li^+ are formed. In these dinitrile-based electrolytes containing extremely high concentrations of Li salt, the proportion of uncoordinated (free) dinitrile solvent become very small, resulting in the high thermal stability of the electrolytes. The self-diffusion coefficients of Li^+, FSA^-, and dinitrile measured with PFG-NMR suggested that Li^+ ion diffuses faster than anion and dinitrile in the liquids of [LiFSA]/[dinitrile] = 1/0.8. In the polymeric network of the solvent- and anion-bridged structures, the translational motions of ligands (solvent and anion) are restricted because each ligand is interacting with multiple Li^+ ions in the highly concentrated electrolytes. However, the Li^+ ion frequently exchanges the ligands (dinitrile and/or anion) in the liquids, and Li^+ ions diffuse faster compared to the ligands. Thus, the hopping conduction of Li^+ occurs through the ligand exchange in the polymeric network structures. Electrochemical measurements clarified that the [LiFSA]/[SN] = 1/0.8 electrolyte possesses a relatively high Li^+ transport ability ($\geq$ 7 mA cm^{-2}) thanks to the Li^+ hopping conduction, regardless of its extremely high viscosity (3142 mPa s) and relatively low conductivity (0.26 mS cm^{-1}) at room temperature. In addition, the [LiFSA]/[SN] = 1/0.8 electrolyte also has a wide electrochemical window, and the graphite anode and $LiNi_{1/3}Mn_{1/3}Co_{1/3}O_2$ cathode of LIBs can be charged and discharged reversibly in this electrolyte.

Conflicts of interest

There are no conflicts to declare.

ACKNOWLEDGEMENTS

This study was supported in part by the JSPS KAKENHI (Grant Nos. 16H06368 and 18H03926 to K. D., 18K14310 to T. M., and 16H06053 to K. U.) from the Japan Society for the Promotion of Science

(JSPS) and the Advanced Low Carbon Technology Research and Development Program (ALCA) of the Japan Science and Technology Agency (JST).

Electronic supplementary information (ESI) available: Crystallographic data, DSC curves. thermogravimetric analyses, Raman spectra, ionic conductivity, viscosity, Walden plot, plots of signal attenuation for ^{1}H, ^{19}F, and ^{7}Li PFG-NMR echo signals, cyclic voltammograms, transference number of Li^{+} ion, and chronoamperogram.

REFERENCES

1 K. Izutsu, *Electrochemistry in Nonaqueous Solutions*, WILEY-VCH Verlag GmbH & Co. KGaA, Weinheim, 2nd edn., 2009.

2 Y. Yamada, K. Furukawa, K. Sodeyama, K. Kikuchi, M. Yaegashi, Y. Tateyama and A. Yamada, *J. Am. Chem. Soc.*, 2014, **136**, 5039–5046.

3 V. Nilsson, R. Younesi, D. Brandell, K. Edström and P. Johansson, *J. Power Sources*, 2018, **384**, 334–341.

4 S. Long, D. R. MacFarlane and M. Forsyth, *Solid State Ionics*, 2003, **161**, 105–112.

5 A. Abouimrane, Y. Abu-Lebdeh, P.-J. Alarco and M. Armand, *J. Electrochem. Soc.*, 2004, **151**, A1028–A1031.

6 P. J. Alarco, Y. Abu-Lebdeh, A. Abouimrane and M. Armand, *Nat. Mater.*, 2004, **3**, 476–481.

7 S. Long, D. R. MacFarlane and M. Forsyth, *Solid State Ionics*, 2004, **175**, 733–738.

8 M. W. Rupich and K. M. Abraham, *J. Electrochem. Soc.*, 1982, **129**, 1857–1861.

9 K. Takada, Y. Yamada, E. Watanabe, J. Wang, K. Sodeyama, Y. Tateyama, K. Hirata, T. Kawase and A. Yamada, *ACS Appl. Mater. Interfaces*, 2017, **9**, 33802–33809.

10 K. Dokko, D. Watanabe, Y. Ugata, M. L. Thomas, S. Tsuzuki, W. Shinoda, K. Hashimoto, K. Ueno, Y. Umebayashi and M. Watanabe, *J. Phys. Chem. B*, 2018, **122**, 10736–10745.

11 S. Kondou, M. L. Thomas, T. Mandai, K. Ueno, K. Dokko and M. Watanabe, *Phys. Chem. Chem. Phys.*, 2019, **21**, 5097–5105.

12 G. M. Sheldrick, *Acta Crystallogr. Sect. A Found. Crystallogr.*, 2015, **71**, 3–8.

13 G. M. Sheldrick, *Acta Crystallogr. Sect. C Struct. Chem.*, 2015, **71**, 3–8.

14 C. S. Johnson, *Nucl. Magn. Reson. Spectrosc.*, 1999, **34**, 203–256.

15 L. M. Smith, A. D. Maher, O. Cloarec, M. Rantalainen, H. Tang, P. Elliott, J. Stamler, J. C. Lindon, E. Holmes and J. K. Nicholson, *Anal. Chem.*, 2007, **79**, 5682–5689.

16 P. Derollez, J. Lefebvre, M. Descamps, W. Press and H. Fontaine, *J. Phys. Condens. Matter*, 1990, **2**, 6893–6903.

17 S. D. Han, J. L. Allen, E. Jónsson, P. Johansson, D. W. McOwen, P. D. Boyle and W. A. Henderson, *J. Phys. Chem. C*, 2013, **117**, 5521–5531.

18 D. M. Seo, P. D. Boyle, J. L. Allen, S. D. Han, J. Erlendur, P. Johansson and W. A. Henderson, *J. Phys. Chem. C*, 2014, **118**, 18377–18386.

19 O. I. Fengler and A. Ruoff, *Spectrochim. Acta, Part A Mol. Biomol. Spectrosc.*, 2001, **57**, 105–117.

20 B. G. Oliver and G. J. Janz, *J. Phys. Chem.*, 1970, **74**, 3819–3822.

21 S. Han, O. Borodin, D. M. Seo, Z. Zhou and W. A. Henderson, *J. Electrochem. Soc.*, 2014, **161**, A2042–A2053.

22 S. Terada, K. Ikeda, K. Ueno, K. Dokko and M. Watanabe, *Aust. J. Chem.*, 2019, **72**, 70–80.

23 S.-A. Hyodo and K. Okabayashi, *Electrochim. Acta*, 1989, **34**, 1551–1556.

24 M. Morita, Y. Asai, N. Yoshimoto and M. Ishikawa, *J. Chem. Soc. Faraday Trans.*, 1998, **94**, 3451–3456.

25 Y. Kameda, Y. Umebayashi, M. Takeuchi, M. A. Wahab, S. Fukuda, S. Ishiguro, M. Sasaki, Y. Amo and T. Usuki, *J. Phys. Chem. B*, 2007, **111**, 6104–6109.

26 M. Yoshizawa, W. Xu and C. A. Angell, *J. Am. Chem. Soc.*, 2003, **125**, 15411–15419.

27 O. Borodin and G. D. Smith, *J. Phys. Chem. B*, 2009, **113**, 1763–1776.

28 C. Zhang, K. Ueno, A. Yamazaki, K. Yoshida, H. Moon, T. Mandai, Y. Umebayashi, K. Dokko

and M. Watanabe, *J. Phys. Chem. B*, 2014, **118**, 5144–5153.

29 Z. Zhang, Y. Shao, B. Lotsch, Y. Hu, H. Li, J. Janek, L. F. Nazar, C. Nan, J. Maier, M. Armand and L. Chen, *Energy Environ. Sci.*, 2018, **11**, 1945–1976.

30 J. Qian, W. A. Henderson, W. Xu, P. Bhattacharya, M. Engelhard, O. Borodin and J. G. Zhang, *Nat. Commun.*, 2015, **6**, No.6362.

31 H. Yoon, P. C. Howlett, A. S. Best, M. Forsyth and D. R. MacFarlane, *J. Electrochem. Soc.*, 2013, **160**, A1629–A1637.

32 X. Fan, L. Chen, X. Ji, T. Deng, S. Hou, J. Chen, J. Zheng, F. Wang, J. Jiang, K. Xu and C. Wang, *Chem*, 2017, **4**, 174–185.

33 P. Zhang, J. Zhu, M. Wang, N. Imanishi and O. Yamamoto, *Electrochem. commun.*, 2018, **87**, 27–30.

34 J. Evans, C. A. Vincent and P. G. Bruce, *Polymer (Guildf).*, 1987, **28**, 2324–2328.

35 J. Newman, K. A. Thomas-Alyea, *Electrochemical Systems, 3rd Edition*, John Wiley & Sons, Hoboken, NJ, 2004.

36 N. P. Balsara and J. Newman, *J. Electrochem. Soc.*, 2015, **162**, A2720–A2722.

37 D. M. Pesko, K. Timachova, R. Bhattacharya, M. C. Smith, I. Villaluenga, J. Newman and N. P. Balsara, *J. Electrochem. Soc.*, 2017, **164**, E3569–E3575.

38 I. Villaluenga, D. M. Pesko, K. Timachova, Z. Feng, J. Newman, V. Srinivasan and N. P. Balsara, *J. Electrochem. Soc.*, 2018, **165**, A2766–A2773.

39 D. B. Shah, H. Q. Nguyen, L. S. Grundy, K. R. Olson, S. J. Mecham, J. M. DeSimone and N. P. Balsara, *Phys. Chem. Chem. Phys.*, 2019, **21**, 7857–7866.

40 K. M. Diederichsen, E. J. McShane and B. D. McCloskey, *ACS Energy Lett.*, 2017, **2**, 2563–

2575.

41 K. Yoshida, M. Tsuchiya, N. Tachikawa, K. Dokko and M. Watanabe, *J. Electrochem. Soc.*, 2012, **159**, A1005–A1012.

42 A. Abouimrane, J. Ding and I. J. Davidson, *J. Power Sources*, 2009, **189**, 693–696.

43 E. Cho, J. Mun, O. B. Chae, O. M. Kwon, H. Kim, J. H. Ryu, Y. G. Kim and S. M. Oh, *Electrochem. Commun.*, 2012, **22**, 1–3.

44 L. Zhang, L. Chai, L. Zhang, M. Shen, X. Zhang, V. S. Battaglia, T. Stephenson and H. Zheng, *Electrochim. Acta*, 2014, **127**, 39–44.

45 Y. Yamada, C. H. Chiang, K. Sodeyama, J. Wang, Y. Tateyama and A. Yamada, *ChemElectroChem*, 2015, **2**, 1687–1694.

Table of Contents Entry

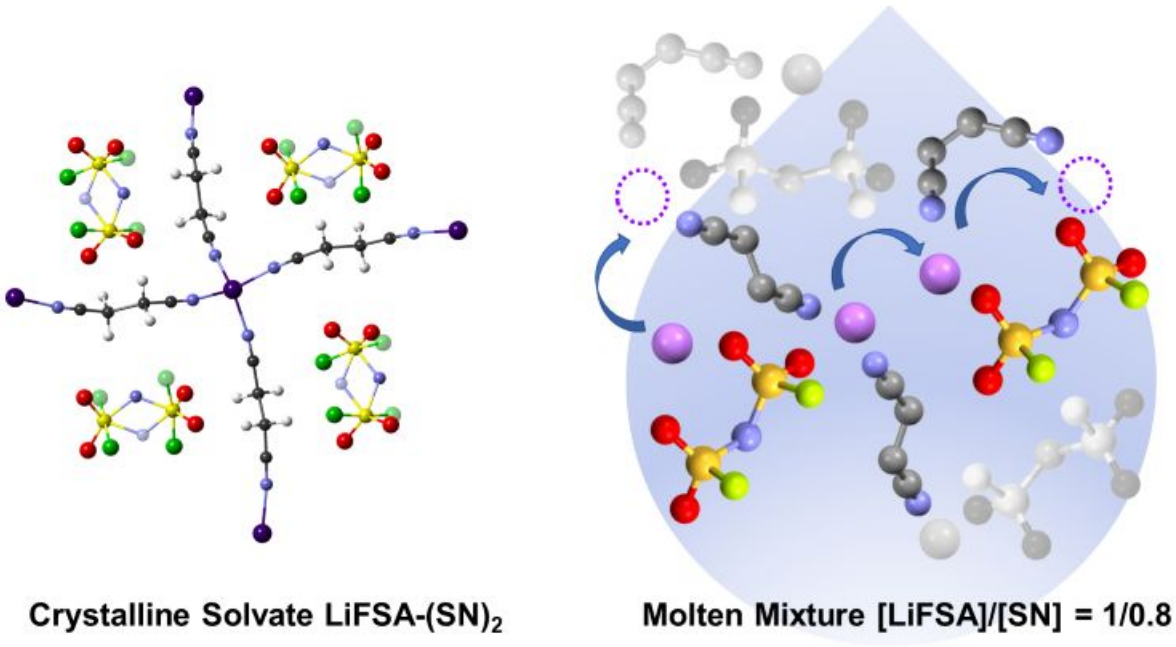

Li^+ ion hopping conduction through ligand (solvent and anion) exchange emerges in solvent-deficient liquid electrolytes of [Li salt]/[dinitrile] > 1.